Electron paramagnetic resonance approaches to study biologically relevant reactions: examples from amyloid aggregation to enzymes

Passerini, L.

Chapter 4.
High-Frequency EPR investigation of a Short-Lived Reaction Intermediate in Small Laccase (SLAC)

A publication of the work described in this chapter is in preparation: L. Passerini, E.J.J. Groenen, M. Huber “High-frequency EPR investigation of a short-lived reaction intermediate in Small Laccase (SLAC)”, to be submitted.

4.1 Introduction

Laccases, or Multi-Copper-Oxidases (MCOs), are a class of multi-domain copper enzymes, which catalyze the oxidation of a variety of substrates coupled to the reduction of molecular oxygen to water [1-6]. Those enzymes play essential roles in all types of organisms, from iron metabolism in humans to lignin degradation in bacteria [1, 2, 7]. Especially bacterial laccases are interesting in industrial applications, due to the broad range of substrates and pH and thermal stabilities [6, 8, 9]. The common feature in MCOs is the presence of at least one of three characteristic copper sites: type-1-Cu (T1Cu), type-2-Cu (T2Cu) and type-3-Cu (T3Cu), each with distinct spectroscopic characteristics. The T1Cu shows a strong absorption at 600 nm in the UV-Vis spectrum, and a copper hyperfine splitting in the parallel direction of 100-180 MHz in the 9 GHz EPR spectrum [10, 11]. The T2Cu does not absorb in the UV, and the EPR spectrum shows a larger hyperfine splitting of 500-600 MHz in the parallel direction [3, 10, 11]. The T3Cu consists of two antiferromagnetically coupled copper atoms, rendering it EPR silent, and shows a weak band in the UV-Vis spectrum at 330 nm [3, 10]. For laccases, the T2Cu and T3Cu are in close proximity, forming the trinuclear cluster (TNC), where oxygen reduction occurs. In 2004, an MCO was isolated, with different architecture than conventional MCOs [12, 13]. This enzyme is a homotrimer with a molecular weight of only 38 kDa, and was named Small LACcase (SLAC) [14].

In figure 1A, the structure of wt SLAC is given, with a focus on the active site [12]. The TNC is situated at the interface between monomers, shown in the figure with different colors.Each monomer contains one T1Cu, and each functional homotrimer contains three active sites.

The reaction between MCOs and oxygen and has been extensively studied [15-20]. We refer to [20] for a comprehensive description of the reaction cycle.

Extensive analysis was performed by EPR spectroscopy on the T1 depleted form (T1D) of SLAC (T1D-SLAC) [20-24]. T1 depletion facilitates the spectroscopic study of the reaction between the TNC and oxygen because it removes the contribution of the strong T1Cu signals from the EPR and UV-Vis spectra. The T1D-SLAC is active in O_2 reduction, provided that reducing agents, such as ascorbic acid [21] or sodium dithionite [23], are added.

In figure 1B the catalytic cycle of T1D-SLAC, with a focus on the TNC, is summarized. As-synthesized, SLAC is in the resting oxidized state (RO). In the EPR spectrum only the T2Cu site is visible, as the T3Cu is EPR silent. In figure SI 1 and SI 5 the EPR spectra of the RO form are shown. Upon reduction, the copper atoms in the TNC are reduced, and all Cu-sites are EPR silent. This is known as the fully reduced state, FR. When the fully reduced protein is mixed with oxygen, the copper sites are reoxidized, and the tyrosine in position 108 is oxidized to form a tyrosyl radical. Here, we refer to this form as the reaction intermediate, RI. The RI

develops on a time scale of milliseconds, and fully decays to the RO state with a half-life of 20 minutes.

In 2009, the intermediate in the reaction between fully reduced T1D-SLAC and oxygen was identified as a copper-tyrosyl exchange-coupled biradical, forming a triplet state [21]. Later, aminoacid substitution studies confirmed the hypothesis of formation of the tyrosyl radical from the residue Y108, situated about 5 Å from the T2Cu [22]. Tyrosyl radicals appear in intermediate states of enzyme reactions for different systems, such as cytochrome oxidase and galactose oxidase [25-31].

Exchange-coupled metal ion-aminoacid radicals were identified in proteins, where they enhance the electron-transfer efficiency in reactions [32]. Studies on synthetic complexes provided insight into metal-radical exchange-coupled systems, showing how the relative orientation and the chemical environment of the involved orbitals can have significant impact on the nature of the coupling [28, 33-35]. For SLAC, the RI-state 9 GHz EPR spectrum revealed that it is a coupled Cu(II)-Tyr-radical system, be it that the magnitude of the exchange coupling could not be determined [24, 36]. Here, we use 275 GHz EPR, which in combination with 9 GHz EPR, enables to determine the exchange coupling. This study contributes to understanding the catalytic cycle of MCOs and the electronic properties of enzyme reaction intermediates, while demonstrating a method for studying short lived reaction intermediates of enzymes by high frequency EPR.

.

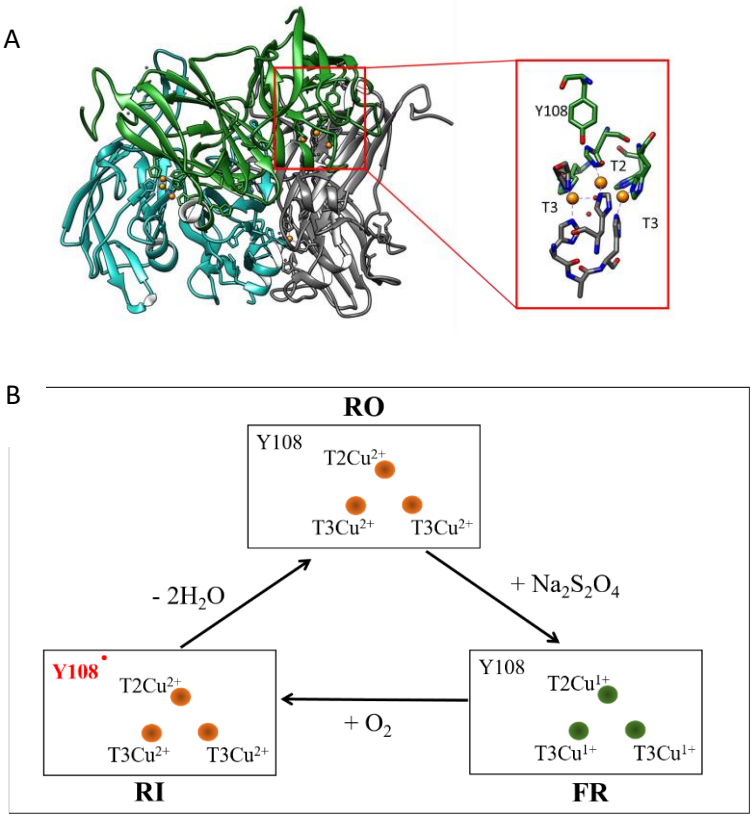

Figure 1. Structure of SLAC (PDB code: 3CG8) and of its oxygen reducing active site (A) and schematic of the reaction cycle at the TNC (B). In A), the three monomers forming the homo-trimer are colored in cyan, grey and green. The active site coppers are coordinated at the interface between monomers. In B), the oxidized copper ions (Cu(II)) are shown in orange, the reduced ones in green. RO : Resting oxidized state, FR: Fully reduced state, RI: Reaction intermediate state.

4.2 Materials and Methods

Protein Expression and Purification

Expression and purification of T1D SLAC was performed as previously described [14], with the only difference consisting in an additional size exclusion chromatography purification step after the anion exchange. The SEC was performed with a HiLoad 16/600, Superdex 200pg column in the same buffer used for elution from the anion exchange step: NaPi 100 mM, NaCl 100 mM, pH 6.8 (preparation buffer). Several batches of protein were prepared to

ensure reproducibility. Three individually prepared batches of protein were measured at 9 GHz and 275 GHz, and more samples of each batch were prepared for 9 GHz EPR measurement (for details, and to see spectra acquired for different batches, see SI).

Preparation for 9 GHz EPR samples

Sample preparation for 9 GHz EPR was performed in inert atmosphere inside a glove box at slight nitrogen overpressure at room temperature. The preparation buffer was exchanged by the nitrogen-saturated measurement buffer (NaPi 100 mM pH 6.8, 20% v/v glycerol) using 30 kDa cutoff amicon filters (Amicon Ultra Centrifugal Filter, 0.5 mL, 30 kDa cutoff, Millipore). The protein was incubated one hour in excess sodium dithionite ($Na_2S_2O_4$ sodium hydrosulphite, Sigma Aldricht) to reduce the copper sites. Desalting steps using 30 kDa amicon filters were done to remove the sodium dithionite from the sample. At this point, the concentrated sample was mixed with a 1:2 volume ratio of oxygen saturated measurement buffer (NaPi 100 mM pH 6.8, 65% v/v glycerol), quickly transferred into a 4 mm external diameter quartz tube and frozen in liquid nitrogen, with reaction times around 40 seconds. The final buffer composition is NaPi 100 mM, pH 6.8, 50% v/v glycerol. The sample was stored in liquid nitrogen until further use. Final protein concentration was in a range between 800 µM to 1 mM.

Preparation for 275 GHz EPR samples

The first step for 275 GHz EPR sample preparation is as described in the section "Preparation for 9 GHz EPR samples". After mixing the reduced T1D SLAC with oxygen saturated buffer, the sample was frozen in liquid nitrogen inside the same Eppendorf tube in which the mixing took place. Less than 30 seconds had passed when the protein and the oxygen saturated buffer were mixed and frozen. The sample was stored in liquid nitrogen until further use. Final sample concentration was in a range between 3 to 5 mM.

Sample transfer in the 275 GHz EPR tubes

Sample preparation is more complicated due to the small dimension of the capillary used at this frequency. To fill the 150 µm internal diameter tubes used for 275 GHz EPR measurements, the procedure described by Panarelli [23, 36] was adapted. The procedure was performed in a polystyrene box under constant flow of cold nitrogen gas, achieved with a N_2 temperature controller (variable temperature unit BVT3000, Bruker BioSpin GmbH), as described in Panarelli [23]. The temperature inside the box ranged between -40 and -15˚C, and was constantly monitored at different positions and heights by using three digital thermometers in combination with the N_2 temperature controller. A 50% v/v glycerol solution has a toothpaste-like viscosity in the temperature range between -30 and -20˚C, and

thereby can be manipulated. The EPR tube was attached to a syringe, and the sample was sucked into the tube by applying under-pressure with the syringe. Once full, the capillary was transferred onto a precooled lab-designed metal block and the sample loaded in the precooled (temperature 200 K) 275 GHz EPR insert with the same procedure as described in [37]. For measurement of the resting state of T1D SLAC, the sample could be manipulated at room temperature, and the sample is drawn in the EPR tube by capillary action.

Continuous wave 9 GHz EPR measurement

9 GHz EPR measurements were performed with an Elexsys E680 X-Band spectrometer from Bruker BioSpin GmbH, equipped with a He-Flow ESR900 cryostat from Oxford instruments. The 9 GHz spectrum was acquired at a temperature of 20 K, with the following parameters : modulation frequency 100 kHz, modulation amplitude 0.5 mT, time constant 327.68 ms, conversion time 81.92 ms, microwave power 20 µW, total measurement time: one hour.

Continuous wave 275 GHz EPR measurements

CW EPR measurements at 275 GHz were performed with a home-built spectrometer described in [38] equipped with a He-flow CF935 cryostat from Oxford instruments, and a laboratory-designed probe head with a single-mode cavity specifically designed for continuous wave measurements [39]. Measurements were performed at a temperature of 10 K, achieved with a continuous He flow. The measurement parameters for the resting-state spectrum are as follows : modulation frequency 1.7 kHz, modulation amplitude 2.4 mT, time constant 300 ms, microwave power: 0.51 µW. Parameters for RI state measurement: modulation frequency 1.7 KHz, modulation amplitude 4.7 mT, time constant 300 ms, microwave power 1.86 µW. The spectrum was acquired in the range between 8 and 11 T. Total measurement time: three to eight hours.

Simulation of EPR spectra

MATLAB (R2019a, The MathWorks, Inc., Natick, MA,USA) and the EasySpin package (5.2.35) were used for simulations of the EPR spectra. Spectra were simulated using the “pepper” function. The parameters used for simulations are listed in table 1. The error margins were generated by manually adjusting the simulation parameters until the simulation visibly differed from the experimental spectrum. The energy level diagrams were simulated with the “levelsplot” function in Easyspin. For a complete picture of the system, simulations were performed for different orientations of the external magnetic field relative to the Cu(II) g-tensor frame. The orientations used were: “x” (θ=90˚, ϕ=0 ˚), “y” (θ=90˚, ϕ=90 ˚), “z” (θ=0˚, ϕ=0˚), and “xyz” (θ=54.74˚, ϕ=45˚) with θ and ϕ as polar angles. In Easyspin the sign of J in $H_{exchange} = J\widehat{\boldsymbol{S}_1}\widehat{\boldsymbol{S}_2}$ is defined such that negative J values correspond to ferromagnetic

coupling (triplet ground state), and positive J values to anti-ferromagnetic coupling (singlet ground state).

4.3 Results

Figure 2 shows the 275 GHz CW-EPR spectrum of the RI state of T1D SLAC, for 9 GHz EPR spectra, see SI. The spectra were obtained by mixing the fully reduced sample with oxygen-saturated buffer (see Materials and methods). Unprocessed spectra, and details about processing, are given in the SI and fig. SI 7. The signal in fig. 2 is composed of two main lines, at 9.6 and 9.7 T. The linewidth of the signals (0.1 T) is such that eventual hyperfine and dipolar interactions remain unresolved. Additionally, broad featureless signals extend in the low field region, between 8.6 and 9.3 T, and could partly derive from background fluctuations, for details see SI. The spectrum is clearly not a superposition of a Cu(II) T2 spectrum and a tyrosyl radical spectrum, revealing that radical–pair interactions, such as exchange coupling J and dipolar interactions **D** play an important role.

To simulate the spectrum, magnetic resonance parameters from 9 GHz EPR, also obtained in this study, are taken into account, resulting in g-tensor (g_{Tyr} and g_{Cu}), hyperfine tensor and dipolar tensor parameters given in table 1.

The 275 GHz spectrum enables to determine the exchange interaction J. To that aim, a series of simulations is performed on the 275 GHz spectrum, see figure 3. Figure 3 shows that positive values of J above 10 GHz introduce intense lines in the high field region, between 10.2 and 10.7 T, see figure 3 A, marked as (2) in figure 3 A and B, that were not seen experimentally, ruling out those values, while values of J between +8 and -16 GHz were ruled out based on the 9 GHz simulations (in figure SI 9 and figure SI 11 the effects of values of J between +8 and -16 GHz on the 9 GHz EPR spectrum are illustrated, and discussed in SI text in “Strategy of simulation of EPR spectra”). As shown in figure 3, only J values between -18 and -19 GHz would provide a simulation that reproduces the experimental spectrum, while for magnitudes of J of -20 GHz or more negative values, there is clear disagreement with respect to the experimental spectrum, because the splitting between the two main signals is too large (compare figure 3 A and C). Therefore, J of the RI state is determined to be between -18 and -19 GHz.

Table 1. Spin Hamiltonian parameters used for the simulation of the SLAC intermediate spectra. The same parameters are used for both the 9 GHz and the 275 GHz simulation. α, β, γ Euler angles, define orientation of **D** relative to **g** and **A** tensor reference frame, using convention by Easyspin [40].

D_{xx} (MHz)	D_{yy} (MHz)	D_{zz} (MHz)	α (deg)	β (deg)	γ (deg)	J (MHz)
300 ± 15	300 ± 15	-600 ± 30	-90	-85	90	-19000 ± 1000

	g_x	g_y	g_z	A_x (MHz)	A_y (MHz)	A_z (MHz)
Copper	**2.042**	**2.052**	**2.26**	**30**	**40**	**626**
Tyrosyl	**2.009**	**2.0043**	**2.002**			

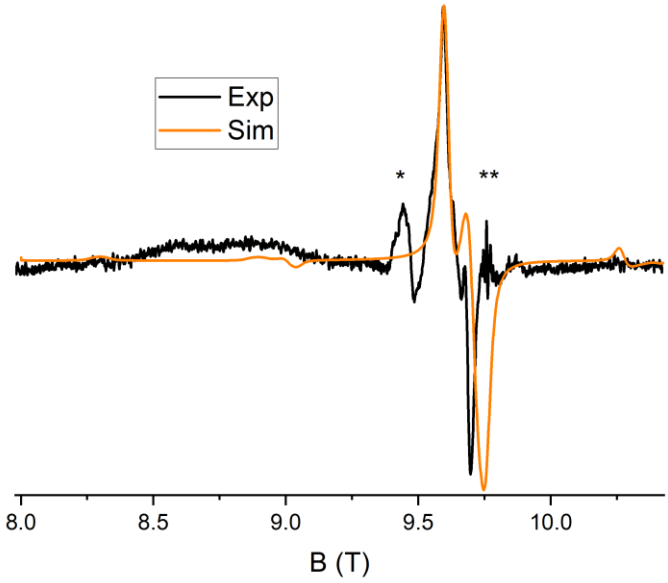

Figure 2. 275 GHz EPR spectrum of the intermediate of T1D SLAC. Black: experimental spectrum, orange: simulation. Experimental spectrum after subtraction of resting state spectrum obtained from the same protein batch. *Residual of resting state spectrum. Shape of resonance at 9.83 T is explained in detail in SI. For details about the subtraction, see fig. SI 7. ** Manganese impurity that overlaps with a radical signal, artifact remains after subtraction. For details about subtraction for the raw, unprocessed spectrum, see SI. Measurement temperature: 10K.

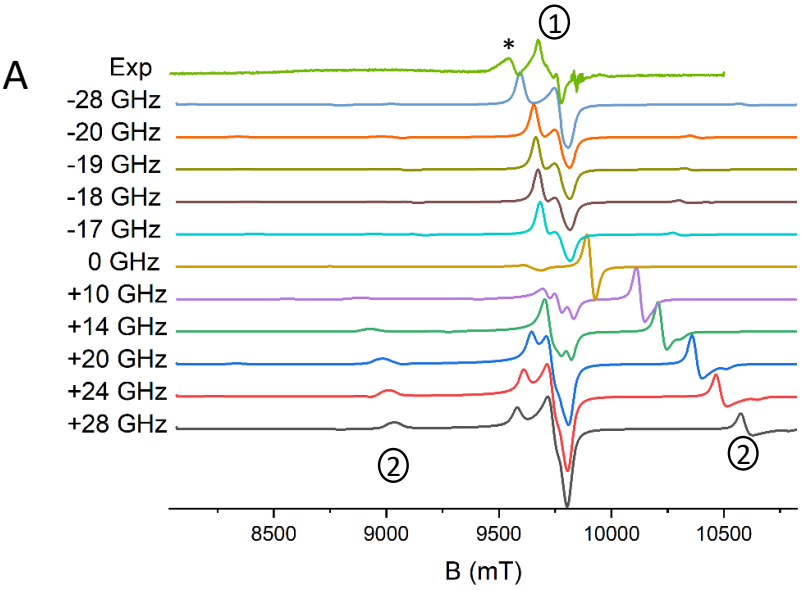
A
Exp
-28 GHz
-20 GHz
-19 GHz
-18 GHz
-17 GHz
0 GHz
+10 GHz
+14 GHz
+20 GHz
+24 GHz
+28 GHz
*
①
②
②
8500
9000
9500
10000
10500
B (mT)

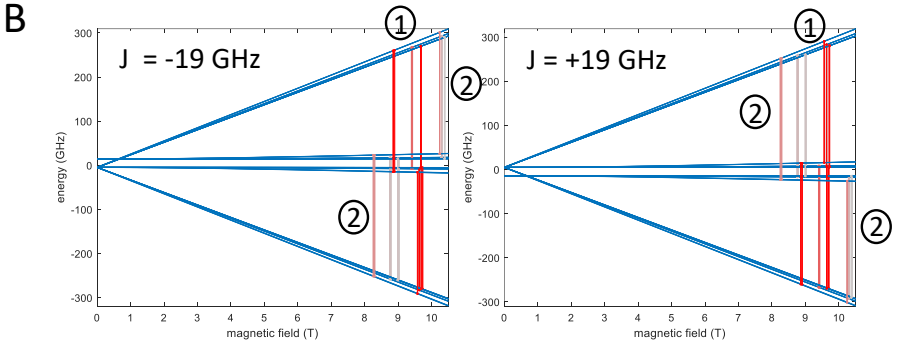
B
J = -19 GHz
J = +19 GHz
①
②
energy (GHz)
magnetic field (T)

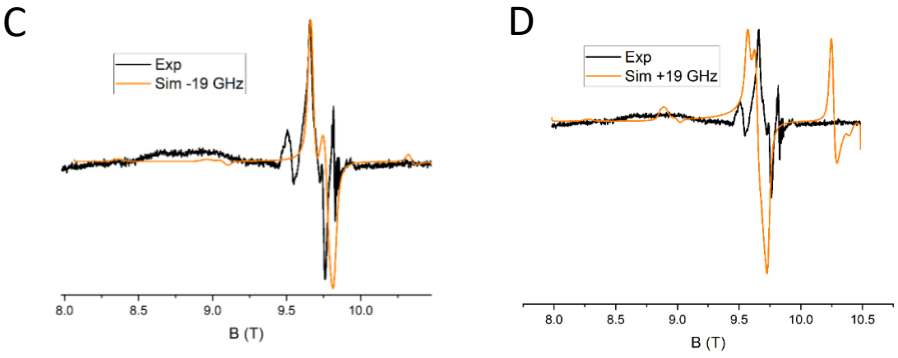
C
Exp
Sim -19 GHz
B (T)
D
Exp
Sim +19 GHz
B (T)

Figure 3. Effect of J on 275 GHz spectra of intermediate. A) Simulation of the 275 GHz spectrum for different values of J. Between 9.5 and 10 T the lineshape is sensitive to the value of J (lines marked 1) and additional transition, with smaller intensity, can occur between 8.5 and 10.5 T, depending on the value of J (lines marked as 2). For a positive value of J, between 10. 5 and 11 T, the transition (2) has much higher intensity for positive than for negative J. For negative values of J, the splitting of the main line increases with an increase of IJI. At J = -28 GHz, the simulation does not reproduce the experimental spectrum anymore. Values of J between 0 and -17 GHz are ruled out by the 9 GHz spectrum simulation, see fig. SI 9 and fig. SI 11. B) Energy levels plot for J = -19 GHz (left) and J = +19 GHz (right). Blue lines: energy levels, the color of the transition lines indicates their probability: red : high, light grey: low (partially allowed). C) and D) Experimental spectrum (black) after subtraction of the resting state is compared with simulation (orange) for C) J = -19 GHz and D) J = +19 GHz. Transition 2: intense lines for J = +19 GHz that are not observed. Those transition are less intense, and hidden in the linewidth, for J = -19 GHz. Asterisks: residual of resting state spectrum. The spectrum shown in C) and D) is shown after subtraction of the resting state contribution, but the manganese and the radical impurity are not subtracted, and evident, at 9.8 T.

4.4 Discussion

The intermediate state of T1D-SLAC (RI state) had been discovered using EPR and UV-Vis spectroscopy in 2009 [21]. The RI state is relatively short lived and is formed when the fully reduced protein is allowed to react with oxygen. This state decays with a half-life of about 20 minutes [21]. The 9 GHz EPR spectra were described as a biradical state, with one electron localized on the CuT2 site and the other on an amminoacid nearby, the Tyr 108 [21]. Here, we determine the EPR parameters of this short lived intermediate with very high field, 275 GHz EPR. The investigation is challenging because to obtain the RI, the reaction is performed in an inert-gas atmosphere, the reaction mixture has to be quickly frozen and kept at low temperature to keep the transformation back to the resting state (RO) of the enzyme at minimum. As RO formation cannot be completely avoided, RI spectra contain a varying fraction of RO state, which is subtracted from the raw spectra (see SI). Similar to previous studies we find variability of resting state (RO) spectra, the origin of which was discussed before and attributed to the presence of two components, which are present in different amounts in different protein batches [20]. In reference [20], the spectra were simulated by two components, showing different degrees of rhombicity and distinct copper g_z values for the two components.

From the combination of 9 and 275 GHz EPR spectra an exchange coupling J of -19 GHz is obtained (see results and SI “Detailed description of the strategy of simulation of 9 and 275 GHz EPR spectra”). With this value of J, now a consistent set of the remaining magnetic resonance parameters of the RI state can be determined. In the SI the steps taken are described in detail, see “Strategy of simulation of EPR spectra”. For a complete list of simulation parameters, see table 1.

The J-coupling observed here can be compared to J-values found for biradicals in biological protein systems and for covalently linked biradicals [25-30, 32-35]. The reported magnitudes of |J| range from 18 MHz [35] to 4800 GHz [34]. The largest J (4800 GHz) is found for a biradical with ten bonds between the radical centers. In enzymatic reactions in proteins, coupled biradicals often involve metal-ion-tyrosyl coupled biradicals [25-30, 33]. In other cases, thiyl- [32] and tryptophan [41] take the role of the tyr in the radical pair. In protein systems, measured |J| values range from 140 MHz [30] to 180 GHz [32]. In these systems the coupling can be ferromagnetic, like in the case of SLAC, or antiferromagnetic, like in the case of galactose oxidase [28, 33].
The J value of the RI in SLAC is in the high range for radical pairs in enzymes, which suggests a relatively strong overlap of the wavefunctions of the T2Cu and the Y108 in the RI state. This could stabilize the intermediate, so the RI could be a key part of the reduction of water to oxygen, and may confirm the role of Y108 in the stabilization of reactive oxygen species formed during the reaction.

The role of the RI state in the reaction of wt SLAC

Is the RI state relevant in the oxygen reduction reaction of wt-SLAC? In [22] the role of Y108 in the wt protein was studied extensively. Substituting Y108 with phenylalanine or alanine did not affect the second-order rate constant (k_{cat}/K_M), indicating that oxygen binding to the active site is unaffected. However, the turnover number (k_{cat}) decreased, suggesting impaired electron transfer to oxygen and a slower reaction than the wt-enzyme when Y108 is knocked out [22]. In the same work, substitution of Y108 led to the disappearance of the spectroscopic signature of the biradical, demonstrating that Y108 is providing the second electron in the RI state, both in the wt and T1D SLAC variants, thus confirming an active contribution of the RI to the reaction mechanism.
With the present study, the 275 GHz EPR spectrum of the RI state is reported. The exchange coupling provides insight into the electronic structure of the biradical and its realitively large value could indicate a role of Y108 in facilitating efficient electron transfer and stabilization of reactive intermediates in the catalytic mechanism of SLAC.

Supplementary Information

9 GHz EPR properties of the RO and the RI state

Figure SI 1 shows variability of RO spectra of different batches, the origin of which is attributed to the presence of different components, showing different rhombicity and different g_z values, present in different amounts in different batches [20]. The spectral part in the g = 4 region (figure SI 3) does not contain an RO contribution but suffers from cavity background.

The 9 GHz EPR spectrum of the RI state (Figure 2) consists of two signals: a more intense $\Delta m_s = 1$ transition (Figure SI 2, SI 4 and SI 12 B) and a weaker, partially allowed $\Delta m_s = 2$ transition (Figure SI 3 and SI 12 A). The $\Delta m_s = 1$ transition exhibits a complex multiline structure, arising from hyperfine and dipolar-coupling-derived splittings. The $\Delta m_s = 2$ transition, also known as the half-field transition, is split into four lines due to hyperfine coupling with the type 2-Cu(II) ion (T2Cu) in the active site, indicating a strongly coupled biradical or triplet (S = 1) state involving Tyr108 (Y108) [21, 22].

The as-measured RI spectrum (Figure SI 2) contains a residual contribution from the resting oxidized (RO) state, which is subtracted as described in Figure SI 4.

Preprocessing of 275 GHz RI spectra

Subtraction of the resting oxidized (RO) state:

It is known that the RI preparation contains some RO state, the amount of which depends on sample preparation details, i.e. mixing and freezing time, and can vary from sample to sample. Therefore, a certain amount of RO spectrum has to be subtracted from the raw RI spectrum. Since the resting state EPR spectrum of different T1D SLAC preparation batches can have different shapes [20], care is taken that for the subtraction, the 275 GHz RO spectrum is from the same batch as the RI preparation batch. There is evidence that the peak at 9.5 T in the RI spectrum (figure SI5) originates from the RO state: the resting-state spectrum has a pronounced peak at 9.5 T, see figure SI 5. Another indication is that in the RI spectra, the relative intensity of the peak at 9.5 T and with respect to the peak at 9.7 T varies for different RI spectra, see fig. SI 6, as expected if the signal at 9.5 T derives from the resting state. Also, the simulations performed, see fig. 3 main text, show that none of the simulations yield spectra with a signal at 9.5 T. Therefore, the amount of resting-state spectrum subtracted from the RI spectra is guided mostly by the amplitude of the 9.5 T peak and considering the overall lineshape, resulting in the spectra shown in figure SI 7. Figure SI 7A shows that the feature at 9.5 T does not exactly overlap in the RI the RO state spectrum. This explains the residual feature at 9.5 T in the processed RI spectrum (figure SI 7C). Also, the

overlap of the RO spectrum and the unprocessed RI spectrum makes the lineshape of the RI spectrum at 9.83 T less reliable than the feature at 9.7 T.
Subtraction of two experimental spectra can add additional line distortions and artifacts to the spectrum. Yet in the present case such artifacts are not obvious and, therefore, no additional baseline correction is performed. To improve the lineshape in the higher field region, a narrow-line radical contribution and the residual six-line pattern of a Mn(II)-impurity are subtracted.

Detailed description of the strategy of simulation of 9 and 275 GHz EPR spectra

As described in [21], the $\Delta m_s=2$ transition of the 9 GHz EPR spectrum is characteristic of a strongly coupled biradical or triplet state. The splitting of this signal into four lines signifies that one of the two unpaired electrons resides on the T2Cu. The second electron was assigned to a tyrosyl radical (Y108)[21]. Thus, the spectra at 9 and 275 GHz were simulated based on two coupled unpaired electrons, one on the T2Cu, and the second on the tyrosyl Y108 radical.
For the interpretation of the spectra, the effect of the magnetic parameters, A_z, **D** and J on the spectra measured at different frequencies need to be considered. For example, while the copper hyperfine and the dipolar interactions are resolved in the 9 GHz spectra, they are masked by the linewidth at 275 GHz. The g-tensor parameters of the Cu(II) T2 are obtained from a combination of 9 and 275 GHz EPR, using characteristic values of T2Cu copper centers [24] and the ones obtained from simulation of RO spectra as starting points. The g-tensor parameters of the tyrosyl radical in the 275 GHz EPR are masked by the effects of the exchange interaction J in the RI state and therefore cannot be extracted from the 275 GHz spectrum of T1D SLAC RI. Therefore, literature values are used [42], and the relative orientation of the g-tensor and the D-tensor cannot be determined.
In the g=2 region, the shape of the 9 GHz EPR spectrum is complicated by overlapping lines arising from a combination of hyperfine and dipolar interactions that have a similar magnitude, see table 1, main text.
However, since the CuT2 hyperfine interaction **A** along the z direction, A_{zCu}, causes the splitting of the $\Delta m_s=2$ transition (g=4) into four lines (see above), it can be measured with high precision. A_x and A_y components of the Cu-hyperfine tensor, with their smaller magnitude, have minimal influence on the overall spectral shape.
The dipolar tensor **D** is estimated from the distance between Y108 and the T2Cu, from the crystal structure of the protein (PDB code: 3CG8), as described in [24], and here is manually adjusted to best fit the simulation to the experimental spectrum.
To evaluate the magnitude of J, various simulation options were explored. Figures SI 8-11 illustrate the effects of different values of J on the 9 GHz spectrum: for values of J between

-16 and 10 GHz, extra lines between 0 and 280 mT occur, fig. SI 9, which do not match the experimental data (see Fig. SI 9 and 10). These additional lines are labelled as transition (3) in figure SI 11. At values of IJI higher than 10 GHz, the g=2 region of the 9 GHz EPR spectrum does not change much, figure SI 8. In the low field region, see figure SI 9, negative values of J between -10 and -16 GHz result in spectra with transitions with an intensity comparable to the half-field $\Delta m_s=2$ signal, which were not observed experimentally, see figure SI 11 for experimental spectra. Thus, values of J comprised between +10 and -16 GHz are excluded. These results enter in the analysis of the 275 GHz spectrum, as described in the main text, from which J = -19 GHz results.

Supplementary Figures

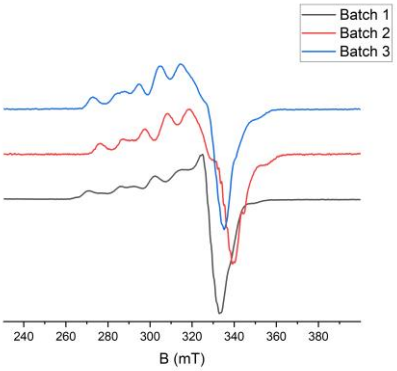

Figure SI 1. Resting state 9 GHz EPR spectra obtained from the different batches of T1D SLAC. Differences in spectra were observed before and attributed to the existence of different components in different ratios, see main text. Measurement temperature: 40K.

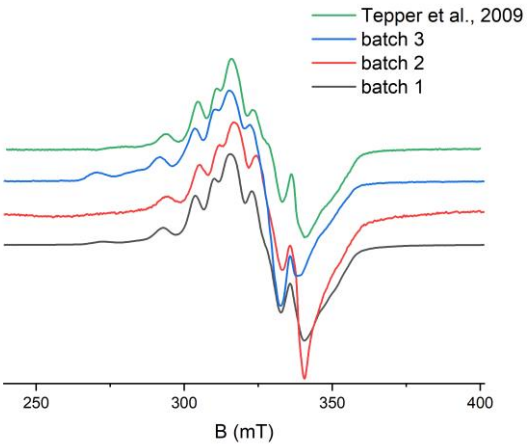

Figure SI 2. 9 GHz EPR RI state spectra as measured, obtained from the different batches of T1D SLAC in the g=2 region. The green spectrum was obtained and published by our group in 2009, and was obtained as described in [21]. Measurement temperature batch 1 to 3: 20K. Tepper et al., 2009 : 40K.

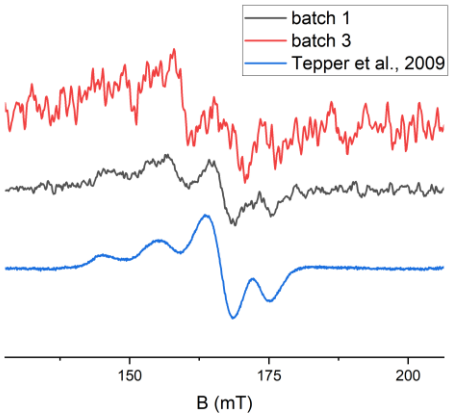

Figure SI 3. Intermediate state 9 GHz EPR spectra obtained from the different batches of T1D SLAC in the $\Delta m_s=2$ region. From batch 1 and 3 no cavity background was subtracted. For simulation the spectrum from Tepper et al., was used for its more reliable lineshape. The $\Delta m_s=2$ spectrum shown in the main text and used for simulation (blue) was published by our group in 2009, and was obtained as described in Tepper et al. [21]. The spectrum from batch 2 (not shown) was obtained on a different spectrometer, and background fluctuations do not allow to interpret this part of the spectrum of batch 2. Measurement temperature batch 1 to 3: 20K. Tepper et al., 2009: 40K.

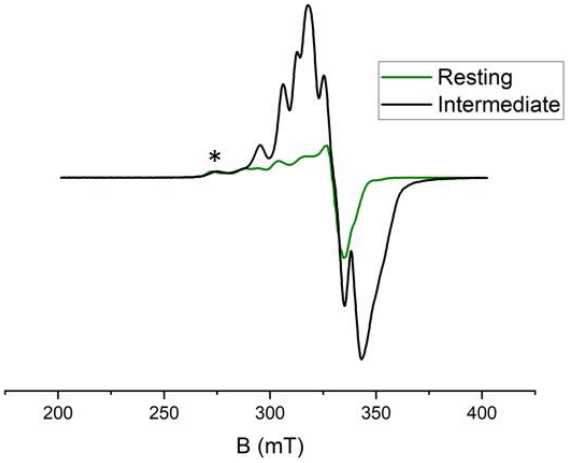

Figure SI 4. Contribution of the 9 GHz RO EPR spectrum on the RI state EPR spectrum of the same batch of SLAC. The spectra were normalized to the low field line of the A_{zz} feature of the Cu-hyperfine interaction of the resting state spectrum, marked by the asterisk. The RI state spectrum shown in the main text figure 2 results from the subtraction of the resting state spectrum (green) from the intermediate state spectrum (black), after the normalization shown in the figure.

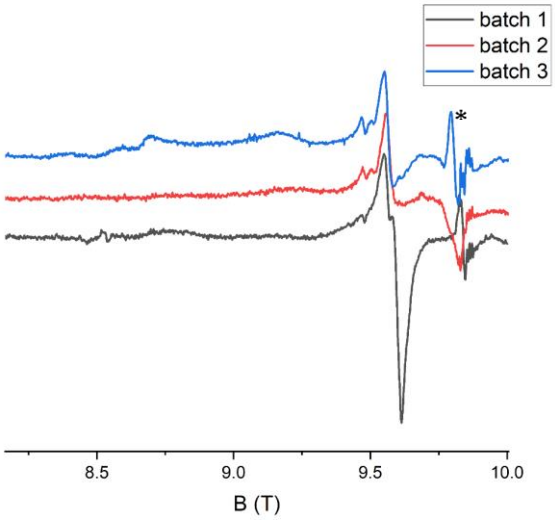

Figure SI 5. Resting state 275 GHz EPR spectra obtained from different batches of T1D SLAC. The spectra show an intense peak in the g_{xy} region (9.6 T). Lines in the g_z region between 8.5 and 9.3 T are broadened and mixed with background fluctuations. In all spectra a six-line manganese (Mn(II)) impurity is present, which overlaps with a signal from another radical contamination, marked by an asterisk. Measurement temperature: 10K.

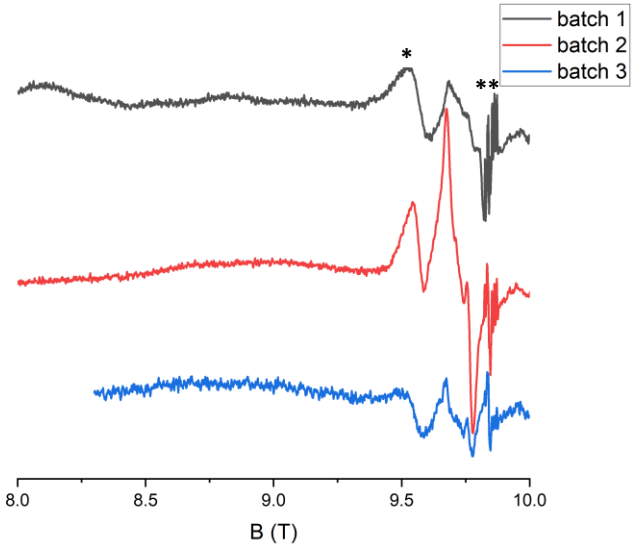

Figure SI 6. Intermediate state 275 GHz EPR spectra from the different batches of T1D SLAC. Shown are raw spectra without background correction and without resting-state subtraction. Marked by *: resting state feature. Marked by **: a six-line Mn(II) impurity, overlapping with a narrow single line radical impurity. The signal at 9.88 T is the least perturbed part the RI spectrum. Spectrum after resting-state subtraction: see figure 3 main text. Protein concentration: 3 to 5 mM. See figure SI 14 for processing steps. Measurement temperature: 10K.

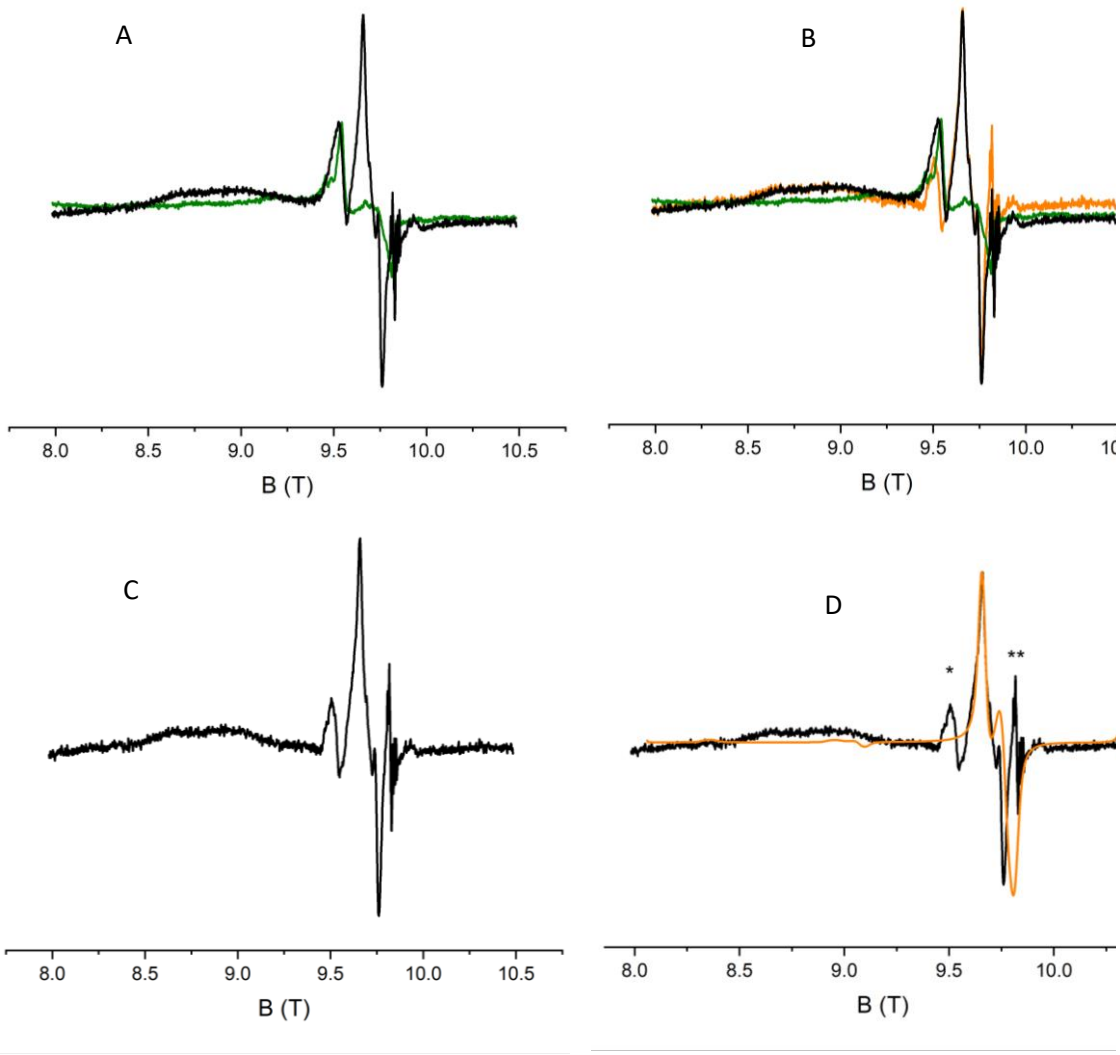

Figure SI 7 Processing of the 275 GHz EPR intermediate spectrum. A) RO spectrum (green), unprocessed RI spectrum (black). B) RO spectrum (orange), RI spectrum (green), result of subtraction (Black). C) Pure intermediate spectrum, resulting from subtraction. D) Pure RI spectrum (black) and simulation (orange). The RI and RO spectra shown are from the same batch. Spectra are normalized to the intensity of the line at B = 9.5 T of the RO state spectrum, and the manganese-impurity signal is used for field calibration of different measurements. * correspond to the residual RO spectrum in the RI spectrum. ** corresponds to the radical and manganese impurities. Artefacts after subtraction are visible in the pure RI spectrum, e.g. narrowing of the higher field line in correspondence to **.

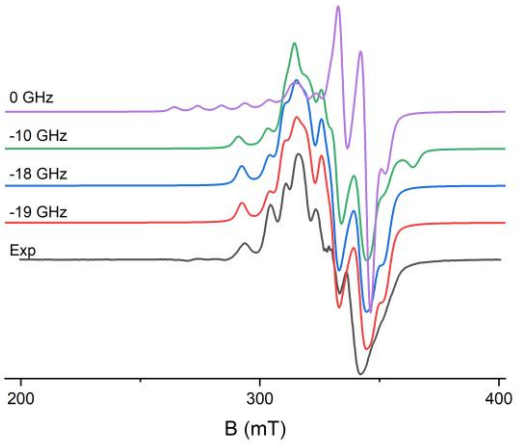

Figure SI 8. Simulated 9 GHz EPR spectra for different exchange interaction (J) values. Spectral shape in the g=2 region. For other simulation parameters see table 1 in the main text.

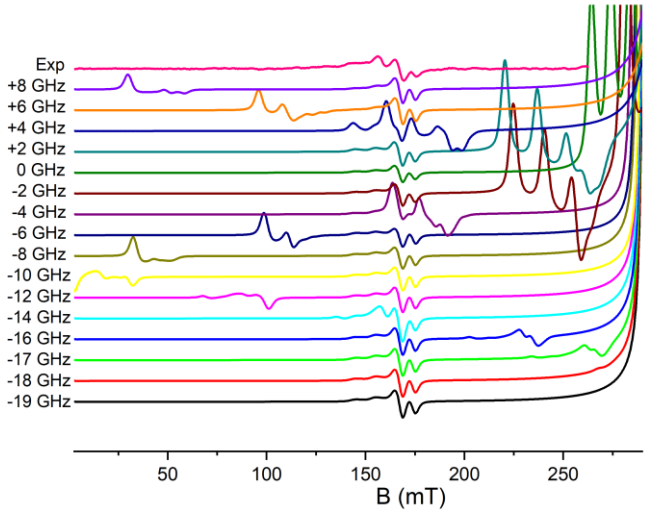

Figure SI 9. Simulated 9 GHz EPR spectra for different exchange interaction (J) values for the low field region of the spectra. Values of J comprised between +8 GHz and -17 GHz imply the presence of additional lines that are not observed experimentally, and are thereby ruled out. For others simulation parameters see table 1 in the main text.

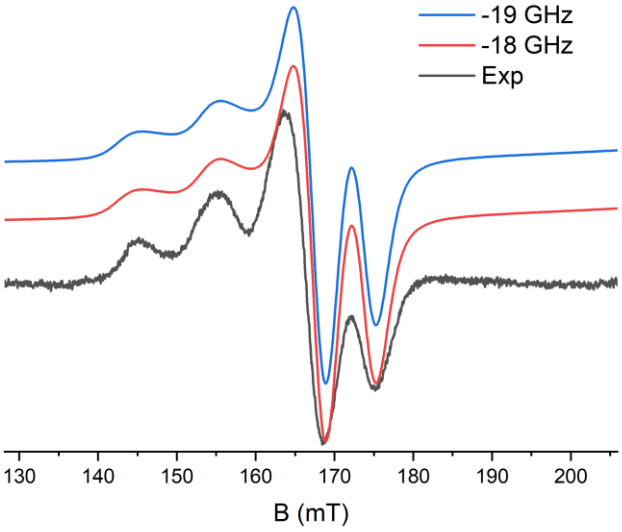

Figure SI 10. Experimental and simulated 9 GHz EPR spectra in the g = 4 region for J = -18 GHz and J = -19 GHz. Experimental spectrum: details, see main text.

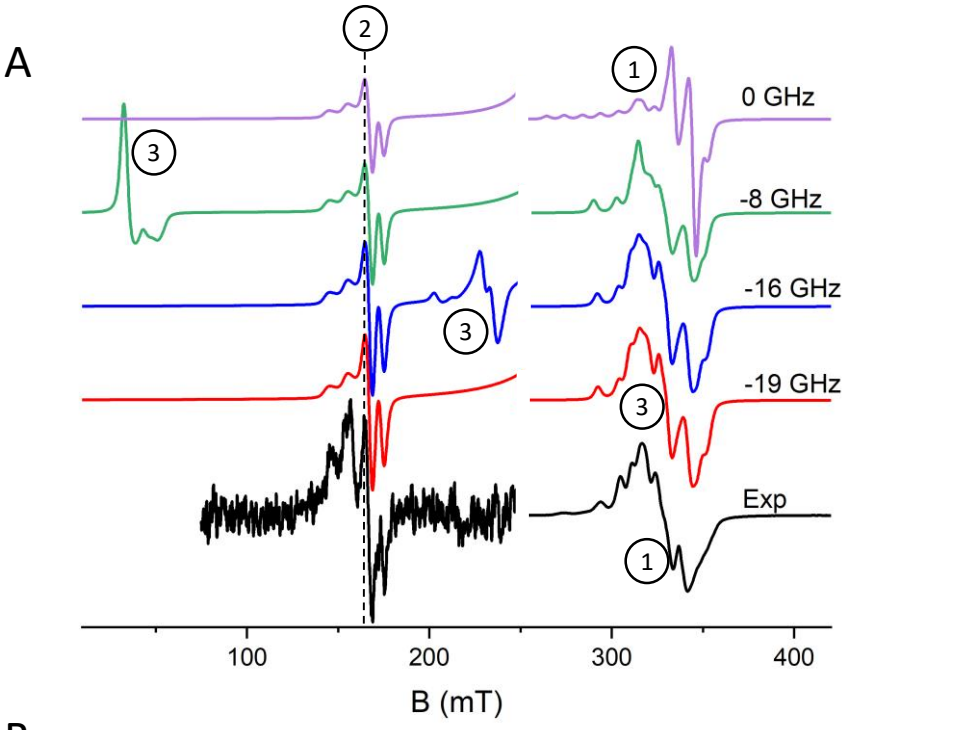
A
2
1
0 GHz
3
-8 GHz
-16 GHz
3
-19 GHz
3
Exp
1
100
200
300
400
B (mT)

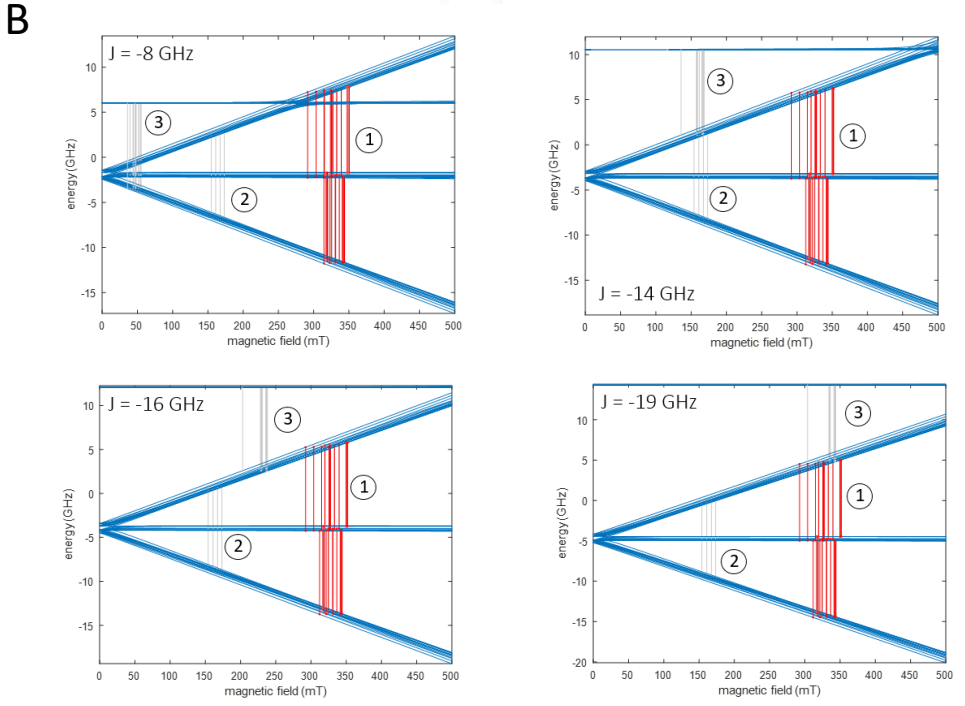
B
J = -8 GHz
J = -14 GHz
J = -16 GHz
J = -19 GHz
energy (GHz)
magnetic field (mT)

Figure SI 11. Effect of J on 9 GHz EPR spectra of the RI state. A) Experimental and simulated 9 GHz EPR spectra for different J coupling values, and B) corresponding energy levels. The amplitude of the low field (0 – 250 mT), $\Delta m_s = 2$ transition, region has been magnified by a factor of 300 for the simulation, and by a factor of 100 for the experimental spectrum. The transitions are numbered in the spectra and in the energy-levels plots : (1) transition giving the g=2 spectrum. (2) $\Delta m_s = 2$ transition, giving the g=4 spectrum. (3) Additional transitions that occur depending on the magnitude of $|J|$. Transition (3) overlaps with transition (2) for J = -14 GHz, and overlaps with transition (1) at J = -19 GHz. Simulation shows that lines marked (3) would appear in the spectrum for J = -8 GHz and J = -16 GHz. Such lines are not observed experimentally, and therefore, those values of J are ruled out (see also fig. SI 11). Blue lines: energy levels, color of the vertical transition lines shows transition probability: red : high, light grey: low (partially allowed).

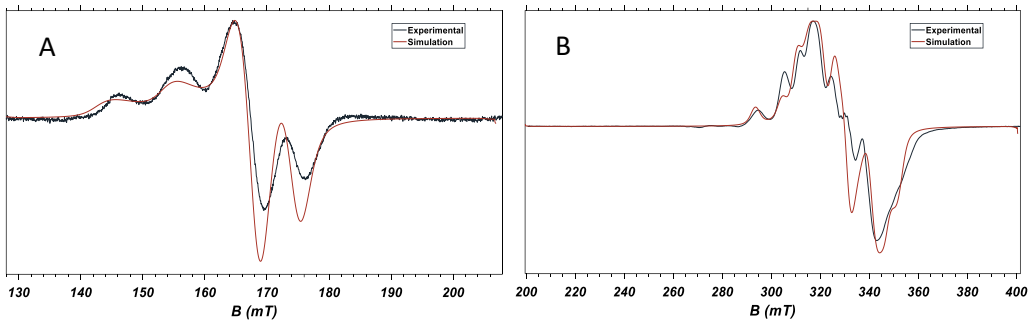

Figure SI 12. 9 GHz EPR spectrum of the reaction intermediate of T1D SLAC. A) Zoom in on the g=4 region, showing the $\Delta m_s = 2$ transition. Black : experimental spectrum, orange: simulation. A) was obtained in our lab and published in Tepper et al., 2009. B). Spectrum in the g=2 region. Black: experimental spectrum, orange: simulation. Simulation parameters: see table 1, main text. Experimental spectrum B) is presented after subtraction of the resting state spectrum obtained from the same protein batch. For details about the processing, see fig. SI 4. Measurement temperature: 20K. Tepper et al., 2009 : 40K.

References

[1] G. Vashchenko, R.T. MacGillivray, Multi-copper oxidases and human iron metabolism, Nutrients 5(7) (2013) 2289-313.
[2] K. Kaur, A. Sharma, N. Capalash, P. Sharma, Multicopper oxidases: Biocatalysts in microbial pathogenesis and stress management, Microbiol Res 222 (2019) 1-13.
[3] E.I. Solomon, A.J. Augustine, J. Yoon, O2Reduction to H2O by the multicopper oxidases, Dalton Transactions (30) (2008) 3921-3932.
[4] K. Obleser, H. Kalaus, B. Seidl, M. Kozich, C. Stanetty, M.D. Mihovilovic, An Organic Chemist's Guide to Mediated Laccase Oxidation, ChemBioChem 23(23) (2022) e202200411.
[5] T. Brugnari, D.M. Braga, C.S.A. dos Santos, B.H.C. Torres, T.A. Modkovski, C.W.I. Haminiuk, G.M. Maciel, Laccases as green and versatile biocatalysts: from lab to enzyme market—an overview, Bioresources and Bioprocessing 8(1) (2021).
[6] I. Bassanini, E.E. Ferrandi, S. Riva, D. Monti, Biocatalysis with Laccases: An Updated Overview, Catalysts, 2021.
[7] G. Janusz, A. Pawlik, U. Świderska-Burek, J. Polak, J. Sulej, A. Jarosz-Wilkołazka, A. Paszczyński, Laccase Properties, Physiological Functions, and Evolution, International Journal of Molecular Sciences, 2020.
[8] M. Sherif, D. Waung, B. Korbeci, V. Mavisakalyan, R. Flick, G. Brown, M. Abou-Zaid, A.F. Yakunin, E.R. Master, Biochemical studies of the multicopper oxidase (small laccase) from treptomyces coelicolor using bioactive phytochemicals and site-directed mutagenesis, Microbial Biotechnology 6(5) (2013) 588-597.
[9] M.u. Rahman, M.W. Ullah, J.A. Shah, S. Sethupathy, H. Bilal, S.A. Abdikakharovich, A.U. Khan, K.A. Khan, N. Elboughdiri, D. Zhu, Harnessing the power of bacterial laccases for xenobiotic degradation in water: A 10-year overview, Science of The Total Environment 918 (2024) 170498.
[10] S.M. Jones, E.I. Solomon, Electron transfer and reaction mechanism of laccases, Cell Mol Life Sci 72(5) (2015) 869-83.
[11] B.G. Malmström, B. Reinhammar, T. Vänngård, Two forms of copper (II) in fungal laccase, Biochimica et Biophysica Acta (BBA) - General Subjects 156(1) (1968) 67-76.
[12] T. Skálová, J. Dohnálek, L.H. Østergaard, P.R. Østergaard, P. Kolenko, J. Dušková, A. Štěpánková, J. Hašek, The Structure of the Small Laccase from Streptomyces coelicolor Reveals a Link between Laccases and Nitrite Reductases, Journal of Molecular Biology 385(4) (2009) 1165-1178.
[13] H. Komori, Y. Higuchi, Structural insights into the O2 reduction mechanism of multicopper oxidase, The Journal of Biochemistry 158(4) (2015) 293-298.

[14] M.C. Machczynski, E. Vijgenboom, B. Samyn, G.W. Canters, Characterization of SLAC: a small laccase from Streptomyces coelicolor with unprecedented activity, Protein Sci 13(9) (2004) 2388-97.
[15] A.E. Palmer, S.K. Lee, E.I. Solomon, Decay of the Peroxide Intermediate in Laccase: Reductive Cleavage of the O−O Bond, Journal of the American Chemical Society 123(27) (2001) 6591-6599.
[16] S. Wherland, O. Farver, I. Pecht, Multicopper oxidases: intramolecular electron transfer and O2 reduction, J Biol Inorg Chem 19(4-5) (2014) 541-54.
[17] J. Yoon, B.D. Liboiron, R. Sarangi, K.O. Hodgson, B. Hedman, E.I. Solomon, The two oxidized forms of the trinuclear Cu cluster in the multicopper oxidases and mechanism for the decay of the native intermediate, Proceedings of the National Academy of Sciences of the United States of America 104(34) (2007) 13609-13614.
[18] J. Yoon, E.I. Solomon, Electronic Structure of the Peroxy Intermediate and Its Correlation to the Native Intermediate in the Multicopper Oxidases: Insights into the Reductive Cleavage of the O−O Bond, Journal of the American Chemical Society 129(43) (2007) 13127-13136.
[19] S.-K. Lee, S.D. George, W.E. Antholine, B. Hedman, K.O. Hodgson, E.I. Solomon, Nature of the Intermediate Formed in the Reduction of O2 to H2O at the Trinuclear Copper Cluster Active Site in Native Laccase, Journal of the American Chemical Society 124(21) (2002) 6180-6193.
[20] R. Dasgupta, K. Gupta, F. Nami, H.J.M. de Groot, G.W. Canters, E.J.J. Groenen, M. Ubbink, Chemical Exchange at the Trinuclear Copper Center of Small Laccase from Streptomyces coelicolor, Biophys J 119(1) (2020) 9-14.
[21] S.M. Armand W.J.W. Tepper, Silvia Sottini, Erik Vijgenboom,, a.G.W.C. Edgar J.J. Groenen, Identification of a Radical Intermediate in the Enzymatic Reduction of Oxygen by a Small Laccase, J. Am. Chem. Soc. 131 (2009) 11680-11682.
[22] A. Gupta, I. Nederlof, S. Sottini, A.W. Tepper, E.J. Groenen, E.A. Thomassen, G.W. Canters, Involvement of Tyr108 in the enzyme mechanism of the small laccase from Streptomyces coelicolor, J Am Chem Soc 134(44) (2012) 18213-6.
[23] E.G. Panarelli, T-Cycle EPR development at 275 GHz for the study of reaction kinetics and intermediates, Doctoral dissertation, Leiden University (2018).
[24] F. Nami, Enzymatic reduction of oxygen by small laccase, a rapid freeze-quench EPR study, Doctoral dissertation, Leiden University (2017).
[25] O. Hansson, B. Karlsson, R. Aasa, T. Vänngård, B.G. Malmström, The structure of the paramagnetic oxygen intermediate in the cytochrome c oxidase reaction, The EMBO Journal 1(11) (1982) 1295-1297-1297.
[26] J.E. Morgan, M.I. Verkhovsky, G. Palmer, M. Wikström, Role of the PR Intermediate in the Reaction of Cytochrome c Oxidase with O2, Biochemistry 40(23) (2001) 6882-6892.

[27] M. Wikstrom, R.B. Gennis, P.R. Rich, Structures of the intermediates in the catalytic cycle of mitochondrial cytochrome c oxidase, Biochim Biophys Acta Bioenerg 1864(2) (2023) 148933.
[28] T.W. Jochen Müller, Eckhard Bill,, L.O.-M. Peter Hildebrandt, a.K.W. Thorsten Glaser, Why Does the Active Form of Galactose Oxidase Possess a Diamagnetic Ground State, Angew. Chem. Int. Ed. 37 (1998) 616-619.
[29] J. Stubbe, P. Riggs-Gelasco, Harnessing free radicals: formation and function of the tyrosyl radical in ribonucleotide reductase, Trends in Biochemical Sciences 23(11) (1998) 438-443.
[30] D.J. Hirsh, W.F. Beck, J.B. Lynch, L. Que, Jr., G.W. Brudvig, Using saturation-recovery EPR to measure exchange couplings in proteins: application to ribonucleotide reductase, Journal of the American Chemical Society 114(19) (1992) 7475-7481.
[31] V.A. Szalai, H. Kühne, K.V. Lakshmi, G.W. Brudvig, Characterization of the Interaction between Manganese and Tyrosine Z in Acetate-Inhibited Photosystem II, Biochemistry 37(39) (1998) 13594-13603.
[32] J. Manzerova, V. Krymov, G.J. Gerfen, Investigating the intermediates in the reaction of ribonucleoside triphosphate reductase from Lactobacillus leichmannii: An application of HF EPR–RFQ technology, Journal of Magnetic Resonance 213(1) (2011) 32-45.
[33] H.L. Achim Sokolowski, R.S. Thomas Weyhermüller, E.B. Eberhard Bothe, Peter Hildebrandt,, K. Wieghardt, Phenoxyl-copper(II) complexes: models for the active site of galactose oxidase, JBIC 2 (1997) 444-453.
[34] P.F. Richardson, R.W. Kreilick, Transition metal complexes with radical ligands: pyridyliminonitroxide radicals with copper and vanadium, Journal of Magnetic Resonance (1969) 29(2) (1978) 285-291.
[35] S.S. Eaton, K.M. More, B.M. Sawant, P.M. Boymel, G.R. Eaton, Metal-nitroxyl interactions. 29. EPR studies of spin-labeled copper complexes in frozen solution, Journal of Magnetic Resonance (1969) 52(3) (1983) 435-449.
[36] E.G. Panarelli, P. Gast, E.J.J. Groenen, Temperature-cycle electron paramagnetic resonance, Physical Chemistry Chemical Physics 22(17) (2020) 9487-9493.
[37] E.G. Panarelli, H. van der Meer, P. Gast, E.J.J. Groenen, Effective coupling of rapid freeze-quench to high-frequency electron paramagnetic resonance, Plos One 15(5) (2020).
[38] H. Blok, J.A.J.M. Disselhorst, S.B. Orlinskii, J. Schmidt, A continuous-wave and pulsed electron spin resonance spectrometer operating at 275GHz, Journal of Magnetic Resonance 166(1) (2004) 92-99.
[39] G. Mathies, H. Blok, J.A.J.M. Disselhorst, P. Gast, H. van der Meer, D.M. Miedema, R.M. Almeida, J.J.G. Moura, W.R. Hagen, E.J.J. Groenen, Continuous-wave EPR at 275GHz:

Application to high-spin Fe3+ systems, Journal of Magnetic Resonance 210(1) (2011) 126-132.
[40] S. Stoll, A. Schweiger, EasySpin, a comprehensive software package for spectral simulation and analysis in EPR, J Magn Reson 178(1) (2006) 42-55.
[41] G. Bleifuss, M. Kolberg, S. Pötsch, W. Hofbauer, R. Bittl, W. Lubitz, A. Gräslund, G. Lassmann, F. Lendzian, Tryptophan and Tyrosine Radicals in Ribonucleotide Reductase: A Comparative High-Field EPR Study at 94 GHz, Biochemistry 40(50) (2001) 15362-15368.
[42] G. Jeschke, EPR techniques for studying radical enzymes, Biochimica et Biophysica Acta (BBA) - Bioenergetics 1707(1) (2005) 91-102.